The Role of Porosity in Filtration

Part XI: Filtration Followed by Expression

This paper addresses the question of the relative amounts of liquid removed during filtration and expression as a function of cake compressibility. As liquid flows through a porous cake, the accumulative drag collapses the particulate structure, thereby increasing the solid content and displacing the liquid. The use of pump pressure in filtration represents the simplest hydraulic deliquoring process. In expression operations, pistons, membranes, rollers, or belts are employed to squeeze the particulate cake after filtration is complete.

Filtration followed by expression at constant pressures ranging from 0.6 to 24.7 MPa (6.1-243.6 atm) was investigated theoretically and experimentally. During filtration and the early stages of expression, the flow rate and average liquid content of highly compressible attapulgite were virtually unaffected by increasing pressure in the range investigated.

F. M. Tiller
Department of Chemical Engineering
University of Houston
Houston, TX 77004

C. S. Yeh
Nelson Industries
P.O. Box 428
Stoughton, WI 53589

Introduction

Reduction of liquid content is important to trucking costs and the landfill characteristics of waste materials. Decreased energy requirements for drying and improved incineration result from lowered moisture fractions. The energy required to express liquid from cakes is negligible compared to the heat required for drying. Consequently, it is desirable to remove the maximum feasible amount by mechanical pressing. Many filters are equipped with membranes for expression. Significant questions include what pressures should be used during filtration and expression to effect the best results. Calculation of the process time required to reach a given average porosity is necessary to design and cycle optimization.

With the advent of tighter controls on the liquid content of wet cakes, solid-liquid separation engineers turned to the use of high filtration pressures. Unexpectedly, increasing pressure failed to increase flow rates sufficiently or to decrease the average liquid content of highly compressible cakes. Filters were then equipped with impermeable membranes to squeeze the cakes. Although expression leads to lower liquid content, the times required for treatment of highly resistant cakes can be substantial.

After a cake is produced by filtration, the liquid is then expressed by the use of mechanical pressure. The final cake structure as characterized by porosity vs. distance represents the initial condition for expression. The assumption that the local flow rate is independent of distance and a function of time alone (equivalent to assuming that the rate of change of porosity with time, $\partial\epsilon/\partial t$, is small) in filtration permits use of ordinary differential equations for determing the relationships among time, filtrate volume, cake thickness, porosity, and pressure. As this assumption is invalid when cakes are squeezed, mathematical solution of the expression process requires a partial differential equation.

Cake compressibility is of paramount significance to filtration and expression behavior. It is characterized by parameters appearing in empirical constitutive equations relating solidosity ϵ_s (volume fraction of solids) and specific flow resistance α to local values of effective pressure. We have chosen power functions of the effective pressures p_s in the forms $\epsilon_s = \epsilon_{so}(1 + p_s/p_a)^{\beta}$ and $\alpha = \alpha_o(1 + p_s/p_a)^n$. When $n > 1$, the material is considered to be highly compressible. In the range for which the constitutive equations are valid, the response to pressure is a strong function of n. As n becomes larger, pressure drop has a decreasing effect on the flow rate and average porosity during filtration. For cakes with $n > 1$, flow resistance increases linearly with the pressure gradient at high pressures. Consequently the flow rate q, which is proportional to the pressure

gradient divided by the flow resistance, approaches a limiting value q_∞.

The ratio $Q = q/q_\infty$ is related to the liquid pressure gradient at the interface between the supporting medium and the cake. When Q reaches some prescribed value (e.g., 0.9), the dimensionless gradient M at the medium will assume a value dependent on Q and n. For the special case in which $n = 2$ and $Q = 0.9$, the dimensionless gradient at the medium has a value of $M = 10$. For a material that is difficult to filter, this gradient could be on the order of 10^6 kPa/m (10^4 atm/m). If the dimensionless gradient were to exceed the value of 10, the rate could increase at most 10%. Conversely if $M \gg 10$ and were decreasing, the flow rate would remain essentially constant until the gradient began to fall below 10.

Our experiments were carried out with large pressure drops, and the liquid pressure gradient at the end of filtration was such that q/q_∞ was close to unity. Consequently, when squeezing started, the rates of expression remained essentially constant until the gradient at the medium dropped to a sufficiently low value. With attapulgite, approximately 80% of the liquid present at the start of expression was removed before the rate began to sensibly decrease.

With highly compressible cakes, a critical region with high pressure gradients is present in those cases in which the filtrate rate has approached a maximum value. Inasmuch as the rate of flow is nearly independent of the pressure gradient in the critical region, it appears that Darcy's law might be invalid. However, the effect of pressure on permeability is such that the product Kdp_L/dx remains constant.

Shirato and his coworkers at Nagoya University have contributed substantially to expression theory; specific citations are made later. This paper extends their work into the region of high pressure and high cake compressibility.

Expression Equipment

Among procedures employed for reducing the liquid content of filter cakes, mechanical expression has achieved prominence in recent years. Squeezing of cakes can be accomplished by several methods including the following, shown in Figure 1:

Roller press (Eimco)

Membrane incorporated inside recessed plate (Lenser America)

Belt press (Williams Jones)

Screw press (NGK Insulators, Ltd., and Fukoku Kogyo Co.)

Hydraulic press applied to horizontal filter (Sanshin Mfg. Co.)

Radial expression in a tube press (English Clays).

The first three operations are carried out continuously. The Sanshin press operates in a semicontinuous manner. A cake produced on a horizontal belt is conveyed to a position under a rectangular press surface. After halting, the expression operation is accomplished while a new cake is being produced. Expression as effected by the last two methods, with hydraulic press or tube press, is batchwise in nature.

The energy used to squeeze liquid out of a cake by mechanical expression is small compared to the thermal energy required for evaporation. With a pressure differential of 10 atm, or about 1,000 kPa, the ratio is 1/400, which shows that the mechanical energy is negligible. Capital and operating expenses of expression equipment determine its cost effectiveness in relation to subsequent processing.

Effect of Stress on Cake Structure

When stress is placed on a cake or sediment, the particulate structure collapses with a resulting decrease in porosity and increase in resistance to flow. The properties of a compressible cake are determined by:

1. The nature of the initial structure laid down under a null stress
2. The change of that structure as loads (frictional drag, gravity, centrifugal force, and boundary stresses due to pistons or membranes) are applied.

In Figure 2 the variation of void ratio e (vol. of liquid/unit vol. of solid) with applied pressures is illustrated for a number of materials with widely different compressibilities. The degree to which mechanical expression can be effective depends upon the difference between the average initial value of the void ratio and the equilibrium value that would be reached under a given applied load. In addition, the variation of permeability with applied load is significant in determining behavior. The materials illustrated in Figure 2 can be classified as follows:

1. Highly flocculated super-compressible structure as illustrated by the polystyrene latex (Grace, 1953)
2. Clay-type structures
   a. Highly compressible attapulgite
   b. Moderately compressible kaolin
3. Insoluble barium sulfate with low compressibility
4. Incompressible crushed limestone.

All of these materials respond in different fashions to pressure in both filtration and expression operations. The flocculated latex possesses a fragile structure that is virtually demolished when the pressure reaches 20–30 kPa. After that it continues as a moderately compressible material similar to the kaolin shown in Figure 2. Whereas flocs of hard particles (spheres as an example) generally collapse easily, clays possess internal strength, which results in a smaller rate of compression at low pressure. Two types of response are illustrated by attapulgite and kaolin in Figure 2. Starting with a null stress void ratio of 10.1 (91% porosity), the attapulgite shows a high degree of compressibility over the entire range of investigation (0–250 atm). The moderately compressible kaolin has a lower null stress void ratio in the range of 2.0–3.0 and provides a structure that is more resistant to change when loaded as compared with the attapulgite. Highly compressible cakes exhibit rapid rises in volume fraction of solids with small increases of pressure. The structural collapse of the cake results in a corresponding rapid decrease in the permeability. When the permeability decreases more rapidly than the first power of the pressure, a material is said to be highly compressible. As will be demonstrated later, such behavior leads to adverse effects in both filtration and expression operations.

Microbarite, which is principally $BaSO_4$ (used in drilling muds), has a low degree of compressiblity. The crushed limestone is typical of irregularly shaped particles which are relatively large and form nearly incompressible beds.

The unstressed structure of a particulate bed can be conveniently characterized by the null stress solidosity (volume fraction of solids) ϵ_{so} and the corresponding permeability K_o. The value of ϵ_{so}, Figure 3, depends upon particle size, shape, and degree of aggregation. For particles with characteristic sizes greater than 10–20 μm, interparticle forces (electrostatic and London-van der Waals) diminish in importance, and the porosity is primarily determined by particle shape. Spherical particles tend toward solidosities of 0.6–0.65, while irregular particles

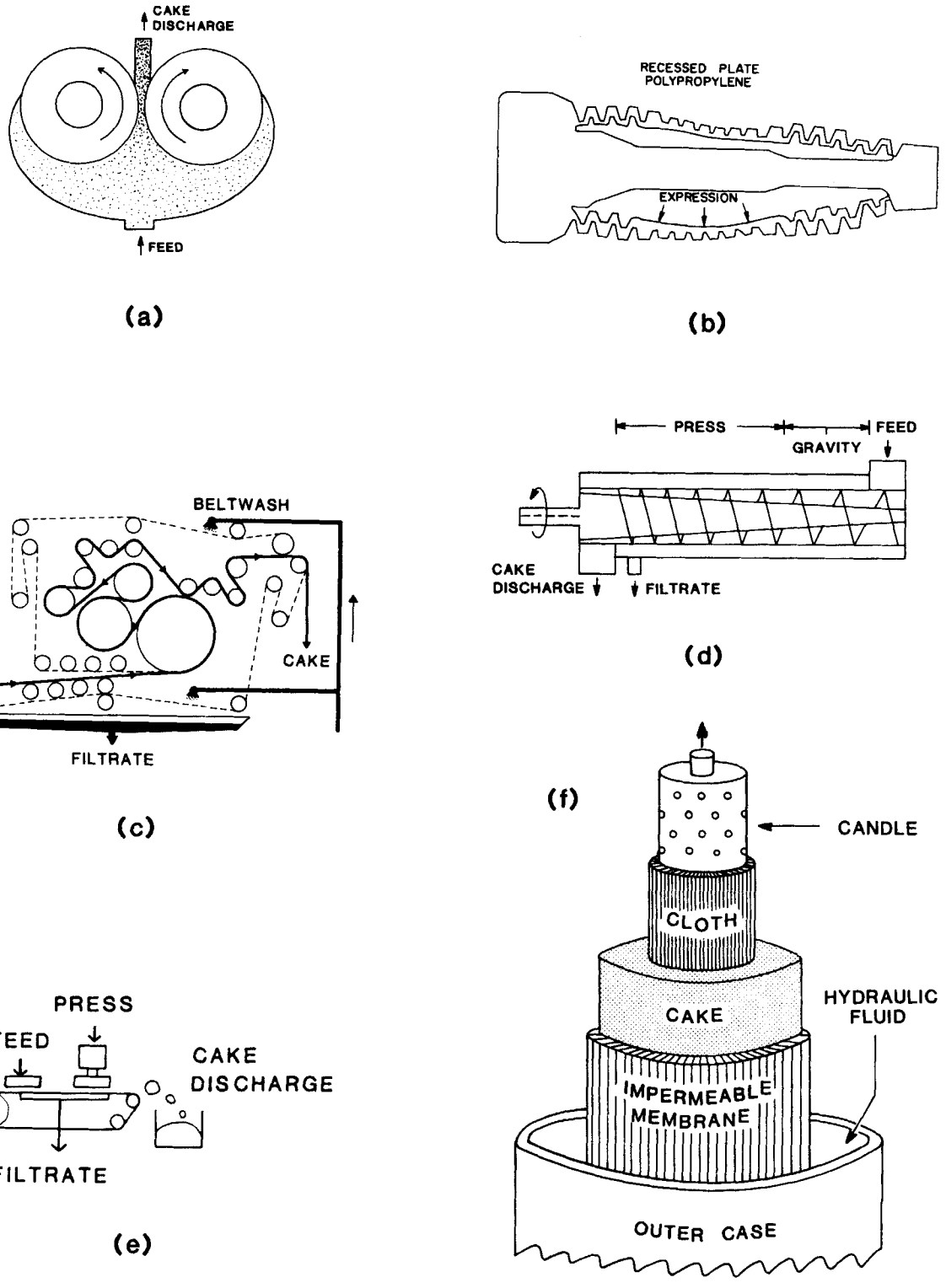

Figure 1. Commercial equipment for mechanical expression.

a. Roller press
b. Membrane incorporated inside recessed plate
c. Belt press
d. Screw press
e. Hydraulic press applied to horizontal filter
f. Tube press for radial expression

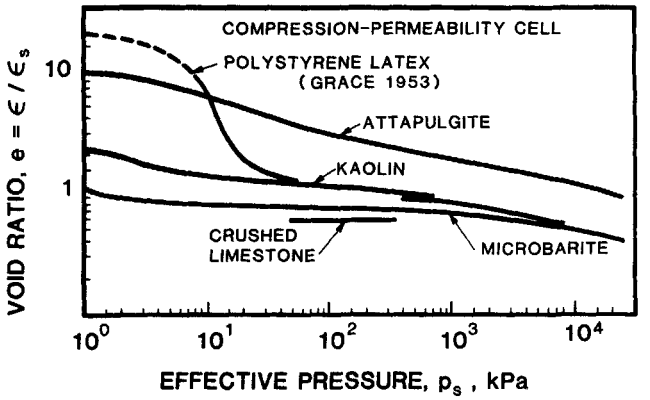

Figure 2. Void ratio vs. applied pressure for materials with different compressibilities.

have more open structures. Filter aids consisting of diatomaceous earth are typical of rugose particles having low solid fractions in the 10–15% range. Inasmuch as cakes with large particles are generally only slightly compressible, they are not good candidates for mechanical expression. Other techniques such as centrifugation, drainage, or blowing can be used to partially eliminate liquid.

The volume fraction of solids of uniform spheres in cubic packing (each sphere is enclosed in a cube having the same diameter) equals $(\pi D^3/6)/D^3 = \pi/6 = 0.524$. The most compact (rhomboherdral) packing yields $\epsilon_s = 0.741$. In either case, the volume fraction of solids is independent of particle diameter. A scanning electron microscope picture of 0.37 μm polystyrene spheres, Figure 4A, shows multiple domains in which the particles have assumed either 60° or 90° arrangements. The domains that correspond to crystalline forms are separated by chaotic arrangements of particles. Solidosities of such beds usually lie halfway between 0.524 and 0.741, e.g., about 0.63 in Figure 4A. Uniform particles do not form uniform structures at the microscopic level (Aksay, 1984). In Figure 3, the horizontal line labeled "Spherical Particles" represents the behavior of compact beds of uniform spheres.

The porosity of beds consisting of particles with characteristic lengths under 10–20 μm depends heavily on the degree of aggregation. As particles decrease in size, interparticle forces become large in comparison to gravitational forces. If the forces are positive, particles stick together in open structures with low solidosities, as illustrated in Figure 4B. Particles with high electrostatic repulsive forces roll over those already laid down rather than adhere at the first points of contact. They then tend to assume a compact arrangement. In Figure 3, the volume fraction of solids for particles under 10 μm is shown to be heavily dependent on the degree of flocculation. As the size diminishes, interparticle forces begin to increase rapidly in comparison to gravitational forces, and aggregate formation becomes possible. The degree of aggregation determines the porosity. For small particles, the volume fraction of solids ϵ_{so} varies through a range of approximately 0.02–0.65. With bimodal distributions or odd shapes, ϵ_s can assume values greater than 0.65. Cakes with low values of ϵ_{so} are excellent candidates for mechanical expression.

Mechanism of Expression

In many particulate separation operations, cake formation is followed by squeezing with a pressure-actuated membrane. In our experiments the combined filtration-expression operation was simulated by filling a cell, Figure 5A, with a slurry and then applying a load through a piston. During the filtration portion of the cycle, the cake grows, and the load is transmitted undiminished through the slurry to the cake surface. Assuming that sedimentation is negligible (a highly questionable assumption; Sambuichi et al., 1982), the slurry concentration remains constant

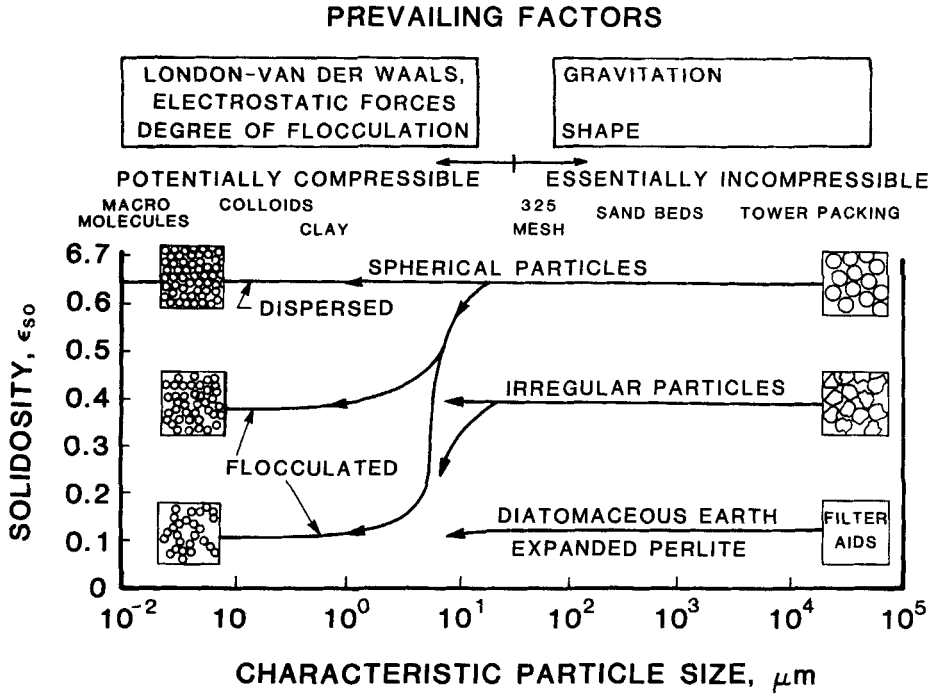

Figure 3. Volume fraction of solids in relation to particle size, shape, and degree of aggregation.

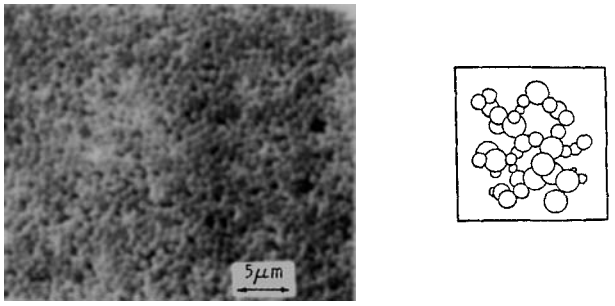

Figure 4. Compact and aggregated sets of particles.

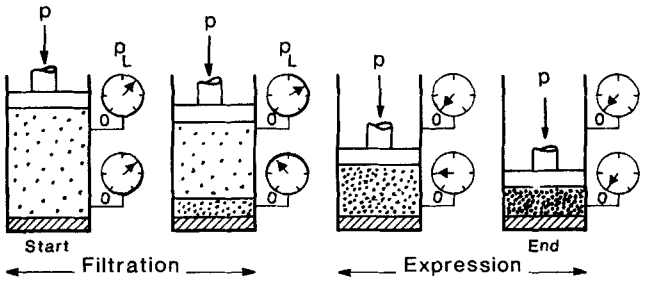

Figure 5. Operation of an expression cell.

throughout the filtration stage, thereby permitting the use of the traditional theoretical approach in estimating flow rate and distributions of porosity and pressure throughout the cake. The cake grows until the slurry disappears, Figures 5B,C, at which point—*A* in Figure 6—the piston contacts the cake surface. Up until that point, $dL/dt > 0$; then when expression starts, dL/dt is negative, leading to a discontinuity in the first derivative. After the piston touches the cake surface, the particulate structure begins to carry an increasing portion of the load and the liquid pressure diminishes. Finally, the cake reaches its equilibrium condition, Figure 5D, and the porosity is uniform throughout the cake (neglecting wall effects, which are important in typical cells regardless of how thin or thick a cake is; Risbud, 1974).

This idealized process is traced in Figure 6 with a three-dimensional diagram. The volume fraction of solids in both slurry and cake is shown as a function of time and distance. Assuming that the supporting medium offers no resistance, the volume fraction of solids is a unique function of the fractional distance through the cake, being ϵ_{so} at the cake surface and ϵ_{sl} at the medium during the filtration period. The volume fraction of solids at the medium remains constant (ϵ_{sl}) during both filtration and expression on the assumption that the medium resistance is negligible. The liquid pressure is zero at the medium, and the full load of the applied pressure is borne by the solids at that point. At the end of the squeezing process when no liquid flow occurs, the solid volume fraction is uniform throughout the cake, as shown by *BB* in Figure 6.

Constitutive Relationships

It is generally assumed that the structure of a compressible, particulate bed subjected to linear compression is a unique function of the initial particle arrangement and the local value of the effective pressure which arises from:

a. Frictional and form drag on particles

b. Surface forces acting through pistons or fluid actuated membranes

c. Centrifugal or gravitational body forces.

Particles are assumed to be in point contact, and internal stresses pass from particle to particle through those contact points. The effective pressure as customarily used in soil mechanics is the sum of the drag, surface, and body forces divided by the total cross-sectional area. As such, it is a superficial or pseudopressure. Interparticle pressures could be infinite if point contact actually existed.

Interparticle forces (London-van der Waals and electrostatic) are of primary importance in determining the initial particle structure but do not enter directly into constitutive equations. The cake structure is characterized macroscopically by permeability K, specific flow resistance α, and solidosity ϵ_s, with only two of the three being independent.

There are no theoretical relations involving the cake structure and effective pressure p_s, and empiricism rules supreme. The authors have employed power functions, polynomials, and exponentials in the general forms:

$$\alpha = \alpha_o f_1(p_s) \quad \text{and} \quad \epsilon_s = \epsilon_{so} f_2(p_s) \tag{1}$$

where $f_i(0) = 1$ and $df_i/dp_s > 0$. In this paper, we choose to use modified power functions (Tiller et al., 1980) as follows:

$$\alpha = \alpha_o(1 + p_s/p_a)^n = \alpha_o(1 + \Pi_s)^n \tag{2}$$

$$\epsilon_s = \epsilon_{so}(1 + p_s/p_a)^\beta = \epsilon_{so}(1 + \Pi_s)^\beta \tag{3}$$

where p_a is an empirical parameter with no physical significance, and $\Pi_s = p_s/p_a$. The permeability is given by

$$K = K_o(1 + \Pi_s)^{-\delta} \tag{4}$$

where $K\alpha\epsilon_s = 1$ and $\delta = n + B$. Because these equations are empirical, they have restricted ranges. As the pressure increases and the cake becomes more compact, the values of n and β vary. Both n and β may change rapidly for highly flocculated materials. For moderately compressible cakes, reasonably accurate

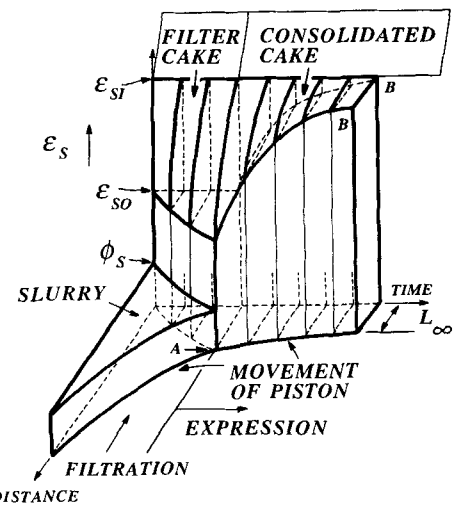

Figure 6. Three-dimensional diagram of an expression process.

values are normally obtained with constant values of the parameters for pressures up to 7–10 atm. In some cases, the range may be considerably extended.

Simultaneous measurement of porosities, flow rates, and pressure gradients at the local level is the ideal procedure for obtaining the parameters in Eqs. 2–4. A number of investigators have obtained liquid pressure profiles, but without simultaneously measuring local porosities (Okamura and Shirato, 1955; Yoshioka et al., 1972; Masterton, 1979; Leu, 1981; Tsai, 1983). Chen (1984) measured both porosity and pressure profiles in sediments subject to gravitational forces where the effective pressures were generally under 10 kPa. Unfortunately, there has been insufficient experimental work to test basic assumptions. Until such time as more fundamental information is available, investigators will have to rely on empirical formulas.

The compression-permeability (C-P) cell (Grace, 1953; Okamura and Shirato, 1955; Tiller et al., 1972; Willis et al., 1974; Okoh, 1977; Willis and Tosun, 1980) has been used by a few investigators to generate porosity-permeability-effective pressure data. It is based on the assumption that a cake has the same porosity and permeability when subjected either to a dead weight stress or to an equivalent accumulative frictional drag. In a C-P cell, a cake is compressed by a piston, and liquid flows through under a very low head so that fluid drag on the particles is small. The permeability and porosity are measured at values of p_s developed by the piston. Risbud (1974) showed that cakes in C-P cells were highly nonuniform and that their accuracy was dubious. Liquid pressures were measured as a function of distance at both the wall and the center of the cell. The pressure was not linear, and permeabilities at the wall were higher than those at the center. Thus a C-P cell yields only approximate values of specific flow resistance and porosity.

There are no completely satisfactory methods for obtaining specific flow resistance. The usual constant-pressure filtration with cake formation on a horizontal surface is seriously affected by sedimentation. Vigorous agitation disturbs the cake surface and does not always cure the sedimentation problem. The authors are unacquainted with any methodology that would permit accurate replication of results in different laboratories. The fickle nature of particulate behavior in slurries also contributes to experimental problems.

Flow Rate Equations

In the conventional use of the Darcy law, it is assumed that the solids are stationary; only the superficial velocity, q, of the liquid appears. However, as expression is accomplished by displacing liquid through movement of the solids into the pores, the velocity of the solids cannot be neglected. In fact, the average superficial velocity of the solids equals the average value of the liquid. For more rigorous calculations, the Darcy equation must be used in the form employed by Shirato et al. (1969):

$$\frac{dp_L}{dx} = \frac{\mu\epsilon}{K}(u - u_s) = \frac{\mu\epsilon}{K}\left(\frac{q}{\epsilon} - \frac{q_s}{\epsilon_s}\right) \tag{5}$$

where x is the distance, u and u_s are average velocities of liquid and solid, and q and q_s are the superficial flow rates.

Equation 5 represents the spatial coordinate form of the Darcy equation and requires measurement of thickness. In many opaque laboratory and industrial cells, there is no instrumentation that permits determinations of thickness, and material coordinates are then favored. As modified by Shirato et al. (1969), the Darcy equation becomes

$$\frac{dp_L}{d\omega} = \mu\alpha\epsilon\left(\frac{q}{\epsilon} - \frac{q_s}{\epsilon_s}\right) \tag{6}$$

where ω is the volume of solids/unit area in distance x and α is the local specific flow resistance based upon solid volume rather than the usual mass/unit area of solids. (The traditional flow resistance used in the literature has been based on the mass of solids/unit area and equals α as defined herein multiplied by the solid density or $\rho_s\alpha$. The units of K and α in this paper are respectively m^2 and m^{-2}. The traditional flow resistance has units of m/kg. In terms of materials normally encountered, α varies from about 10^{13} for filter aids to 10^{17} m^{-2} for colloidal particles.) The two coordinates are related by

$$d\omega = \epsilon_s dx \tag{7}$$

and $K\alpha\epsilon_s = 1$. The porosity ϵ appears on the outside of the brackets in Eqs. 5 and 6 because of the manner in which the permeability was originally defined. When $q_s = 0$, the righthand sides of Eqs. 5 and 6 reduce to the standard Darcy form $\mu q/K$ or $\mu\alpha q$.

Willis and Tosun (1980) claimed that the flow resistance α may be a double-valued function and therefore that the material coordinate form of the Darcy-Shirato equation should be avoided. However, they failed to realize that the permeability and porosity are properties of sets of particles that are characterized by moving material coordinates. Cake properties accompany the material as it moves and are not generally functions of position in space. We have encountered no data for real materials in which the spatial and material coordinate forms of Darcy's equation yield different results. Smiles (1970, 1978, 1982) and Schiffman et al. (1986) emphasized the necessity of expressing the permeability in Darcy's law in terms of flow relative to the solid particles rather than fixed spatial coordinates.

Stress Balance

Stress on the solids is derived from accumulative frictional drag during filtration; during expression it is generated by drag plus the direct load of the piston on the particulates. With negligible inertial effects, a force balance over a portion of the cake between an arbitrary distance x and the surface at $x = L$, Figure 7, leads to

$$F_s + Sp_L = Sp \tag{8a}$$

where F_s = accumulative stress on the particles, S = cross-sectional area, and p = pump-generated pressure at the cake surface during filtration and piston pressure during expression. In our work, p is the same for both processes. Equation 8A requires that the liquid pressure be effective over an unbroken but wavy, fictitious membrane at every point in the cake. The particles must be in point contact if p_L is to act over the entire surface and if $\int p_L \vec{n} dS$ is to be replaced by Sp_L. Dividing Eq. 8a by the area results in

$$p_s + p_L = p \tag{8b}$$

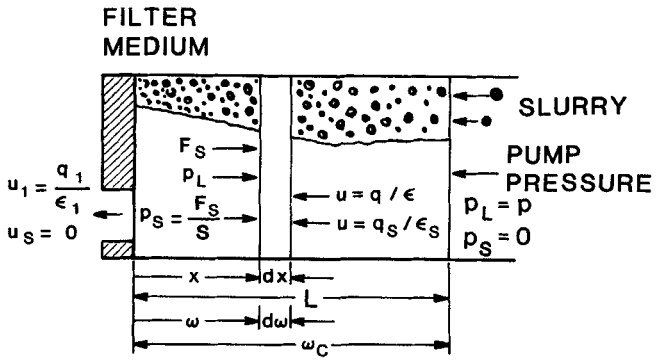

Figure 7. Diagram of a filter cake.

The effective pressure p_s represents the sum of stresses resulting from the frictional drag on all of the particles plus the load on the piston divided by the cross-sectional area. It is a pseudopressure used for convenience in constitutive relationships. As piston pressure is increased to high values, point contact among particles would be expected to change into area contact (Tiller and Huang, 1961). At the present stage of development, there is insufficient information available to warrant changes in Eq. 8. Further research is needed to develop new insight into the effect of high stresses on particulate structures.

The hydraulic pressure p_L and the effective pressure p_s are functions of either (x, t) or (ω, t), whereas the applied pressure is either constant or a function of time. At a fixed time, taking a differential of Eq. 8 yields $dp_L = -dp_s$. The differential of the hydraulic pressure in the Darcy equation can then be replaced by dp_s. As the constitutive equations relate α, K, ϵ, and ϵ_s to p_s, elimination of p_L is required for subsequent integrations of the resulting equations.

Quasi Steady-State Approximation for Filtration

Combination of the Darcy equation with differential material balances leads to nonliner partial differential equations. We shall make a quasi steady-state assumption that is expected to be accurate for filtration and approximate in the initial stage of expression. A material balance over both liquid and solid for the cake lying between the medium $x = 0$, and distance x yields, Figure 7:

$$q + q_s = q_1 \tag{9}$$

where q_1 is the exit flow rate/unit area of the filtrate. Eliminating q_s from Eqs. 5 and 6 and replacing dp_L by $-dp_s$ leads to

$$\frac{dp_s}{dx} = -\frac{\mu q_1}{K}\left(\frac{q/q_1 - \epsilon}{1 - \epsilon}\right) \approx -\frac{\mu q}{K} \tag{10}$$

$$\frac{dp_s}{d\omega} = -\mu\alpha q_1\left(\frac{q/q_1 - \epsilon}{1 - \epsilon}\right) \approx -\mu\alpha q \tag{11}$$

If $q/q_1 \approx 1$ as occurs in the filtration of dilute to moderately concentrated slurries (Tiller and Shirato, 1964), the terms in brackets in Eqs. 10 and 11 reduce to unity. For filtration we shall assume they are unity and recognize that a small error is involved. Then the superficial flow rate q is constant through the cake and equal to q_1.

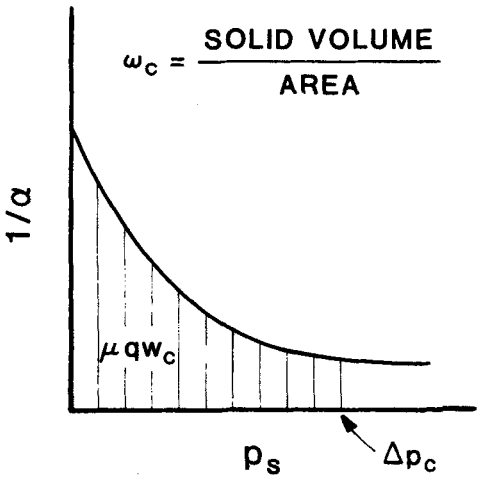

Figure 8. $1/\alpha$ vs. p_s.

Average Porosity at End of Filtration

Equations 10 and 11 can be placed in forms for integration by solving for Kdp_s and dp_s/α. Then an integration across the cake yields

$$\mu qL = \int_0^{\Delta p_c} K dp_s = \int_0^{\Delta p_c} dp_s/\alpha\epsilon_s \tag{12}$$

$$\mu q\omega_c = \int_0^{\Delta p_c} dp_s/\alpha \tag{13}$$

The term qL is called the rate-thickness product. As $\omega_c = \epsilon_{sav}L$, dividing Eq. 13 by Eq. 12 gives

$$\epsilon_{sav} = \int_0^{\Delta p_c} dp_s/\alpha \Big/ \int_0^{\Delta p_c} dp_s/\alpha\epsilon_s \tag{14}$$

Subject to the simplifications involved, the average solidosity ϵ_{sav} is a unique function of Δp_c. Graphical interpretation of Eqs. 12–14 is illustrated in Figures 8 and 9. The first graph shows a plot of $1/\alpha$ vs. p_s. The area under the curve between $p_s = 0$ and Δp_c (pressure drop across the cake) corresponds to $\mu q\omega_c$, where ω_c is the volume per unit area of solids in the cake. The second graph

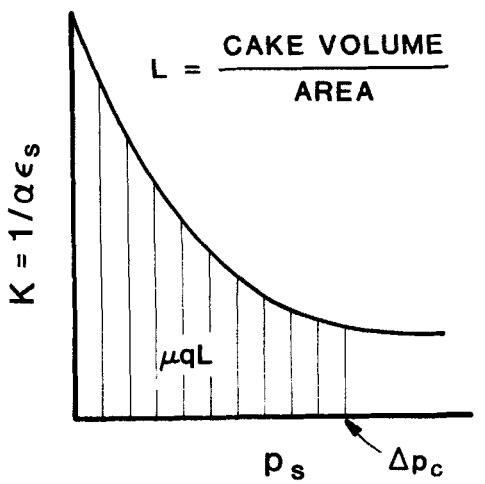

Figure 9. K vs. p_s.

is a plot of K or $1/\alpha\epsilon_s$ vs. p_s. Each point in the proceeding graph is divided by ϵ_s, and the area under this curve equals μqL where L is the cake thickness or total cake volume per unit area. Dividing the area in the first graph by the area in the second graph gives the average volume fraction of solids. Under the assumed conditions, ϵ_{sav} remains constant as long as Δp_c does not change; the rate drops inversely with cake thickness. In normal industrial practice, this approximation would be expected to be valid when the cake thickness exceeds about 4–5 mm and the cake formation time is 10–15 min or longer. Then the medium resistance would be small, and most of the pressure drop would be consumed by the cake.

The actual shape taken by the curves in Figures 8 and 9 determines the behavior of cakes in relation to applied loads. We shall discover some startling differences in behavior of moderately and highly compressible materials.

Substitution of Eqs. 2 and 3 into Eq. 14 produces

$$\epsilon_{sav} = \epsilon_{so}\frac{(1-\delta)}{(1-n)}\left[\frac{(1+\Delta\Pi_c)^{1-n}-1}{(1+\Delta\Pi_c)^{1-\delta}-1}\right] \tag{15}$$

where $\Delta\Pi_c = \Delta p_c/p_a$. Two limiting forms of this equation are of importance. First, when $\delta < 1$, the numerator increases more rapidly than the denominator as Δp_c becomes larger, and ϵ_{sav} increases. For moderate values of δ less than approximately 0.5–0.6 and high values of Δp_c, the final 1 can be dropped in the numerator and denominator, leading to the useful approximation

$$\epsilon_{sav} = \epsilon_{so}\frac{(1-\delta)}{(1-n)}(1+\Delta\Pi_c)^{\beta} \tag{16}$$

Within the normal range of filtration pressures up to 5–10 atm, Eq. 16 predicts an increasing solids content as the pressure drop across the cake rises.

For highly compressible cakes with $\delta > 1.0$ and $n > 1.0$, Eq. 15 can be placed in the form

$$\epsilon_{sav} = \epsilon_{so}\frac{\delta-1}{n-1}\left[\frac{1-1/(1+\Delta\Pi_c)^{n-1}}{1-1/(1+\Delta\Pi_c)^{\delta-1}}\right] \tag{17}$$

As Δp_c becomes large, Eq. 17 approaches

$$\epsilon_{sav} = \epsilon_{so}(\delta-1)/(n-1) \tag{18}$$

Thus, we find that a highly compressible material does not respond as expected to increasing pressure. The explanation of this anomaly lies in the formation of a dense skin close to the medium that adsorbs most of the pressure drop and leaves a large fraction of the cake unconsolidated (Tiller and Green, 1973; Tiller and Horng, 1983). These equations must be viewed with caution for materials with δ greater than approximately 0.7. The empirical constitutive Eqs. 2–4 are only valid for limited pressure ranges that are quite narrow for many highly flocculated materials. Only qualitative conclusions can be drawn from the equations when n is variable. Nevertheless if n is variable and greater than unity, it can be shown by using Eq. 14 that a limiting volume fraction of solids is reached as pressure increases.

Rate as a Function of Δp_c

The rate-thickness qL and rate-volume of solids per unit area $q\omega_c$ products as given by Eqs. 12 and 13 become

$$\mu qL = \frac{K_o p_a}{1-\delta}[(1+\Delta\Pi_c)^{1-\delta}-1] \tag{19}$$

$$\mu q\omega_c = \frac{p_a}{\alpha_o(1-n)}[(1+\Delta\Pi_c)^{1-n}-1] \tag{20}$$

We are interested in these expressions for highly compressible materials with n and δ greater than unity. As Δp_c becomes indefinitely large, the products become

$$\mu q_\infty L = K_o p_a/(\delta-1) \quad \delta > 1 \tag{21}$$

$$\mu q_\infty \omega_c = p_a/\alpha_o(n-1) \quad n > 1 \tag{22}$$

In using these equations, it is necessary to recognize that $\omega_c = \epsilon_{sav}L$. The rate approaches a limiting value q_∞ and essentially becomes independent of the pressure drop. Using the expression in Eq. 22 involving cake volume the ratio of q/q_∞ for constant ω_c becomes

$$Q = q/q_\infty = 1 - 1/(1+\Delta\Pi_c)^{n-1} \tag{23}$$

A plot of Q is shown in Figure 10 for values of n ranging from 1.1 to 2.0. Although n's do not necessarily remain constant for highly compressible particulate structures, the curves show qualitatively the behavior expected as pressure is increased.

Average values of permeability and flow resistance are defined by

$$K_{av} = \frac{1}{\Delta p_c}\int_0^{\Delta p_c} K dp_s = \frac{K_o p_a}{(1-\delta)\Delta p_c}[(1+\Delta\Pi_c)^{1-\delta}-1] \tag{24}$$

$$\frac{1}{\alpha_{av}} = \frac{1}{\Delta p_c}\int_0^{\Delta p_c} dp_s/\alpha \tag{25}$$

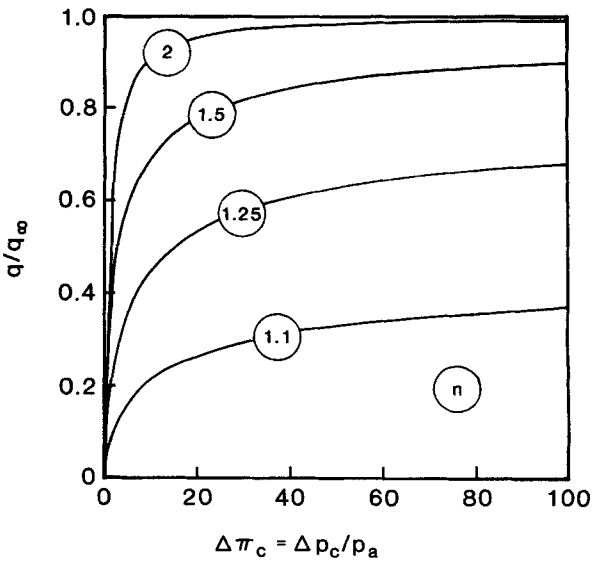

Figure 10. $Q = q/q_\infty$ vs. Π_c.

[The average value as defined by Eq. 25 has been used in filtration and centrifugation theory for many years. Mathematically the result should be written as $(1/\alpha)_{av}$, which does not equal $1/\alpha_{av}$. The usual equations become somewhat clumsy if we use $(1/\alpha)_{av}$, and we maintain customary practice.]

The reciprocal of Eq. (25) is

$$\alpha_{av} = \alpha_o (1 - n) \frac{\Delta\Pi_c}{(1 + \Delta\Pi_c)^{1-n} - 1} \tag{26}$$

Just as the rates approached limiting values, the average permeability and average specific flow resistance also assume special forms for highly compressible cakes; thus Eqs. 24 and 26 become

$$K_{av} = K_o p_a / (\delta - 1)\, \Delta p_c \tag{27}$$

$$\alpha_{av} = \alpha_o (n - 1)\, \Delta p_c / p_a \tag{28}$$

It can be seen that the average permeability decreases inversely with Δp_c, while the average specific flow resistance is directly proportional to the pressure drop for highly compressible cakes under high pressures. Assuming that the medium resistance is negligible, the rate is given by $q = \Delta p_c / \mu \alpha_{av} \omega_c$, leaving the rate independent of Δp_c. We shall use this information in dealing with both high-pressure filtration and expression.

Hydraulic Pressure Distribution

Integration of Eq. 11 subject to $q/q_1 = 1$ and negligible medium resistance yields the following relationships for the hydraulic pressure distribution and the dimensionless value of the pressure gradient with respect to the volume of solids/unit area at the medium where $\omega = 0$:

$$\Omega = \omega/\omega_c = 1 - \frac{(1 + \Delta\Pi_c - \Pi_L)^{1-n} - 1}{(1 + \Delta\Pi_c)^{1-n} - 1} \tag{29}$$

where

$$\Pi_L = p_L/p_a \text{ and } \Pi_L/\Delta\Pi_c = p_L/\Delta p_c$$

then

$$\left[\frac{d(\Pi_L/\Delta\Pi_c)}{d\Omega}\right]_{\Omega=0} = M = \frac{Q}{n-1}\left[\frac{1}{1 - Q - (1 - Q)^{n/(n-1)}}\right] \tag{30}$$

For the special case of $n = 2$, Eq. 30 becomes

$$M = 1/(1 - Q) \tag{31}$$

When Q reaches 90% of its ultimate value, the dimensionless slope M has a value of 10, and the dimensionless pressure drop $\Delta\Pi_c = 9$, a relatively low value. In Figure 11 the dimensionless pressure Π_L is plotted against the dimensionless material coordinate Ω for $n = 2$ at different values of $\Delta\Pi_c$. Curve A shows the Π_L distribution for $\Delta\Pi_c = 9$. At the origin the slope is $M = 10$. For curve B with $\Delta\Pi_c = 50$, the slope at the origin is 50. In spite of the fivefold increase in M, the rate only rises about 8%. When the gradient reaches values in excess of those shown for curve B,

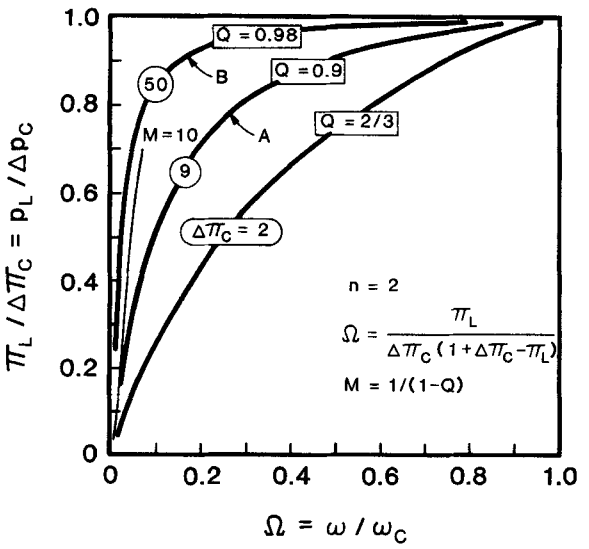

Figure 11. Π_L vs. ω/ω_c.

a type of criticality is reached in which the flow rate no longer responds to changes in the gradient.

Comparison of Expression and Filtration

Differences are expected between the squeezing action of a piston on moderately and highly compressible cakes. A comparison of the effect of pressure on the removal of liquid with filtration and expression is illustrated in Figure 12. The void ratio, which represents the volume of liquid per unit volume of solid, is plotted as a function of the pressure drop for highly compressible attapulgite, and moderately compressible microbarite (principally $BaSO_4$). The attapulgite first forms a cake having a low null stress solid volume fraction of $\epsilon_{so} \approx 0.09$ (void ratio = 11.1). Attapulgite filter cakes are formed with average porosities of 0.78–0.80, corresponding to void ratios of 4.0–4.5. Although a substantial amount (60%) of the initial liquid is removed by filtration, little improvement is brought about by pressures above 2 atm and as high as 250 atm. Such behavior is in accord with the limiting average volume fraction of solids predicted by Eq. 18. If a squeezing process is applied to the attapulgite filter cake, additional quantities of liquid can be removed, as shown by the lower curve marked "Expression" in Figure 12. An additional 30% of the liquid could be removed over and above that taken out by pressure filtration at a pressure equal to 24.7 MPa (244 atm) provided the process were continued until equilibrium was established.

The null stress void ratio, $e \approx 2.0$–3.0, of microbarite is much lower than the corresponding value for attapulgite, and its more compact structure offers less opportunity for substantial liquid removal.

Quantitative Approach to Expression

Determination of the local ϵ_s as a function of distance and time requires solution of the partial differential equation (PDE) governing flow through compressible, particulate structures subject to the initial conditions imposed by cake formation during filtration. In our work we shall accept the results for filtration based upon the quasi steady-state model to provide initial conditions for the PDE. Although the PDE should be used for

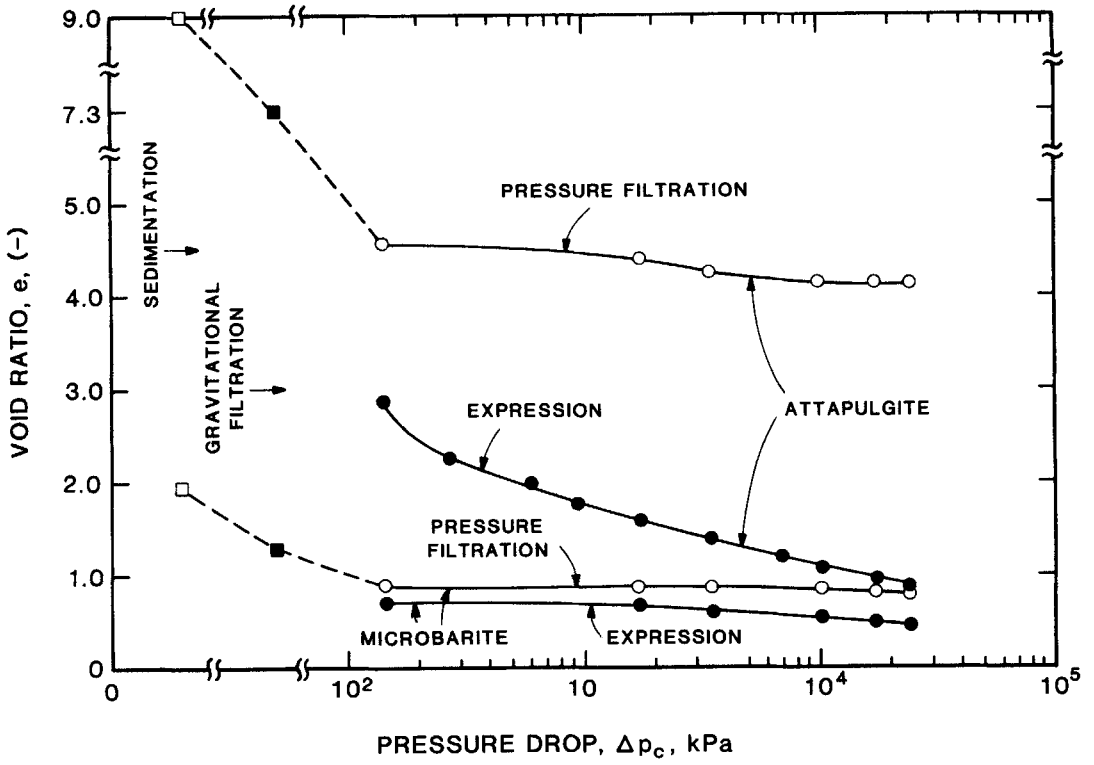

Figure 12. Average void ratio vs. pressure drop in filtration and expression.

the filtration phase, our experience indicates that nothing would be gained in accuracy or practicality by employing it instead of the more conventional equations.

A major difference between the mathematical treatment of filtration and expression involves the solid velocity u_s, which was neglected in comparison with the liquid velocity during filtration. As the liquid movement during expression is entirely due to displacement by the solid, it is not possible to neglect u_s.

Derivation of the PDE's for expression requires that the equation of continuity be combined with the Darcy-Shirato equation. In spatial coordinates, the equation of continuity takes the form

$$\left(\frac{\partial q}{\partial x}\right)_t = -\left(\frac{\partial q_s}{\partial x}\right)_t = \left(\frac{\partial \epsilon}{\partial t}\right)_x = -\left(\frac{\partial \epsilon_s}{\partial t}\right)_t = -\frac{d\epsilon_s}{dp_s}\left(\frac{\partial p_s}{\partial t}\right)_x \tag{32}$$

In material coordinates, the equation of continuity becomes

$$\left(\frac{\partial q}{\partial \omega}\right) = -\frac{1}{\epsilon_s}\left[q_s\left(\frac{\partial \epsilon_s}{\partial \omega}\right)_t + \left(\frac{\partial \epsilon_s}{\partial t}\right)_\omega\right] = -\frac{d\ln\epsilon_s}{dp_s}\left[q_s\left(\frac{\partial p_s}{\partial \omega}\right)_t + \left(\frac{\partial p_s}{\partial t}\right)_\omega\right] \tag{33}$$

It should be noted that $q_s = (\partial\omega/\partial t)_x$.

To obtain the differential equations governing flow through compressible, particulate structures, we solve for q in Eqs. 10 and 11, differentiate with respect to x or ω, and set the results equal to Eq. 32 or 33. For spatial coordinates, there results

$$\frac{\partial^2 p_s}{\partial x^2} + \frac{d\ln(K\epsilon_s)}{dp_s}\left(\frac{\partial p_s}{\partial x}\right)^2 + \frac{\mu q_1}{K}\frac{d\ln\epsilon_s}{dp_a}\frac{\partial p_s}{\partial x} - \frac{\mu}{K}\frac{d\ln\epsilon_s}{dp_s}\frac{\partial p_s}{\partial t} = 0 \tag{34}$$

This equation involves the flow rate q_1 at the medium. A similar procedure followed in developing the corresponding equation in material coordinates results in:

$$\frac{\partial^2 p_s}{\partial \omega^2} - \frac{d\ln\alpha}{dp_s}\left(\frac{\partial p_s}{\partial \omega}\right)^2 - \frac{\mu\alpha}{\epsilon_s}\frac{d\ln\epsilon_s}{dp_s}\frac{\partial p_s}{\partial t} = 0 \tag{35}$$

This equation is free of q_1 and is preferred by the authors for solution of the expression equations. The derivative $\partial p_s/\partial t$ is at constant ω in Eq. 35, whereas it is at constant x in Eq. 34. Changing Eq. 35 to dimensionless form yields

$$\frac{\partial^2 \Pi_s}{\partial \Omega^2} - \frac{d\ln A}{d\Pi_s}\left(\frac{\partial \Pi_s}{\partial \Omega}\right)^2 - \Delta\Pi_c\frac{A}{E}\frac{d\ln E}{d\Pi_s}\frac{\partial \Pi_s}{\partial T} = 0 \tag{36}$$

where $\Pi_s = p_s/p_a$, $\Omega = \omega/\omega_c$, $A = \alpha/\alpha_o$, $E = \epsilon_s/\epsilon_{so}$, and $T = \Delta p_c\epsilon_{so}t/\mu\alpha_o\omega_c^2$. In the work that follows, the medium resistance will be neglected and Δp_c will be replaced by the applied pressure p.

Expression is assumed to start at the moment filtration ceases. Thus the Π_s vs. Ω relation holding at the end of filtration represents the initial condition for expression and takes the

form

$$\omega/\omega_c = \Omega = 1 - \frac{(1 + \Pi_s)^{1-n} - 1}{(1 + \Delta\Pi_c)^{1-n} - 1} \tag{37}$$

Two boundary conditions are needed. At the piston, the velocities of the solid and liquid are equal. Consequently, as there is no relative motion and $u_s = u$, the pressure gradients of both p_s and p_L are zero. At the medium, we assume that $p_L = 0$ and $p_s = p$. Thus the boundary conditions can be summarized as at $\Omega = 1$, $d\Pi_s/d\Omega = 0$; at $\Omega = 0$, $\Pi_s = 1$.

Shirato et al. (1970) numerically solved the transient expression problem using a different set of constitutive equations. Risbud (1974) solved the PDE using a finite-difference approach with initial cakes having uniform structures. Our work differs principally in consideration of the relation between filtration and expression and in the range of compressibilities. Numerical solution of Eq. 35 was accomplished using the method of weighted residues involving orthogonal collocation (Villadsen and Michelsen, 1978). Details of the procedure are available in the dissertation by Yeh (1985).

Application of the method to real systems requires knowledge of parameters in the constitutive equations. Experimental reproducibility of the empirical parameters is a continuing problem. At present, they are primarily obtained from constant-pressure filtration experiments or from compression-permeability cells. Although the latter device is flawed, the authors used it to obtain data for attapulgite and microbarite in the range up to 24.7 MPa. Unfortunately, data obtained directly from traditional constant-pressure filtration experiments are also frequently flawed due to such problems as sedimentation (Sambuichi et al., 1982), continued clogging of the medium, bed collapse by sudden application of the full pressure, and disintegration of aggregates. Data used for obtaining the parameters involved in Eqs. 2 and 3 for attapulgite are shown in Figure 13. Although neither precise nor accurately reproducible, the data provide a reasonable base for an approximate comparison of theory and experiment.

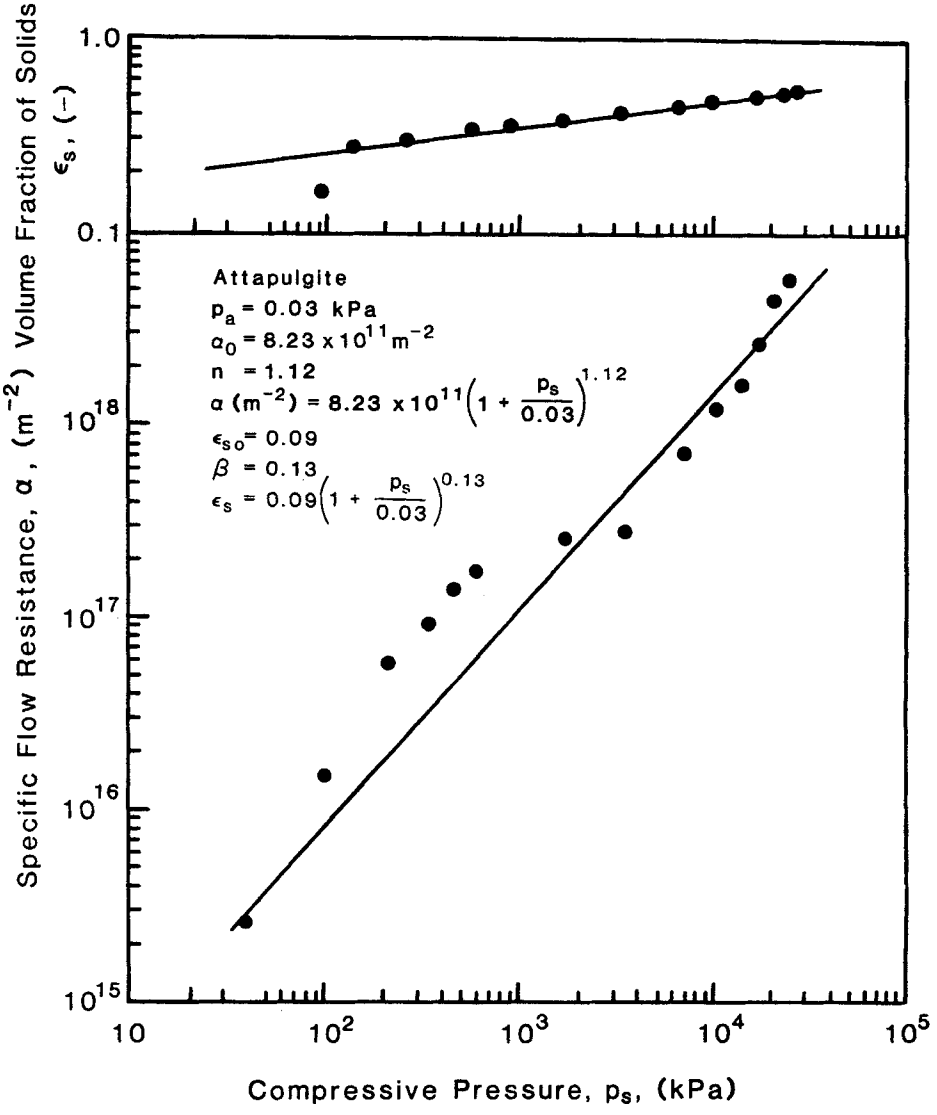

Figure 13. α and ϵ_s vs. p_s for attapulgite.

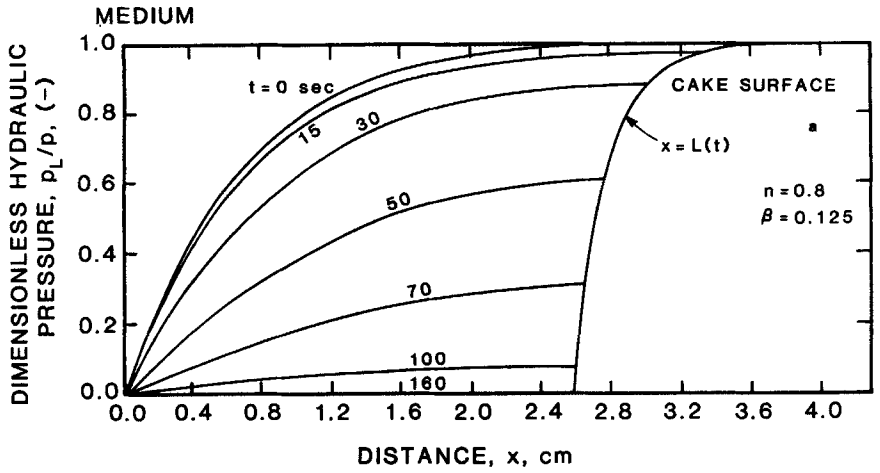

Figure 14a. Hydraulic pressure distribution in expression of a very compressible material.

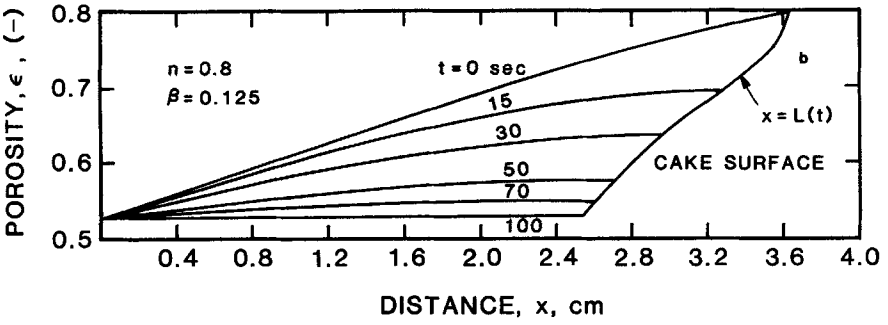

Figure 14b. Porosity distribution in expression of a very compressible material.

At the very high piston pressure involved in the C-P cell, the usual procedure of using a low liquid head of less than 1 m of fluid to obtain α would have yielded about 0.1 mL/day of water. Even with a pump that operated around 0.7–1.0 MPa, the flow rate was barely in a measurable range.

Porosity and Pressure Distribution

In Figures 14 and 15, calculated results are shown for two model materials having high and very high compressibilities. The parameters used are:

	α_o, m^{-2}	n	ϵ_{so}	β	P_a, Pa	R_m, m^{-1}
Figure 14	2.5E14	0.8	0.2	0.125	5.0	E10
Figure 15	2.5E15	1.2	0.1	0.2	5.0	E11

Parameters having the same values were $\mu = 0.001$ Pa · s, $P = 5$ MPa, and $\omega_c = 0.012$. After calculations were made on the basis of material coordinates, the results were changed to spatial coordinates in order to illustrate the change of cake thickness with time. The larger curvature of both p_L and ϵ vs. x at the medium in Figures 15a, b as compared to Figures 14a, b illustrates the effect of compressibility. The expression time is on the order of 10^2 s for the less compressible material, and 10^2 min for the more compressible material.

Experimental Study of Mechanical Expression

Filtration and mechanical expression experiments were carried out in a mechanism similar to that shown in Figure 5 (Yeh, 1985). An expression cell made of alloy steel with 4.0 in (101.6 mm) ID and 0.5 in (0.13 mm) wall thickness was used with the mechanical force being supplied by a 30 ton hydraulic press that gave a maximum pressure of 33 MPa. A floating-type bottom piston permitted measurement of the transmitted force. The cake was compressed by the top piston, and the liquid was squeezed out through the bottom porous piston. Whatman No. 1 filter paper was used as a medium to prevent clogging of the porous support.

We define ϵ'_{av} as the volume of liquid in the cell divided by the volume between the top piston and the medium. The quantity ϵ'_{av} is the average porosity of both slurry and cake during the filtration period; ϵ'_{av} equals the average porosity of the cake, ϵ_{av}, during the consolidation period.

In Figure 16, combined filtration and expression data for microbarite are shown for pressures ranging from 1.7 to 24.7 MPa. The rapid drop of the piston was due to the low resistance of the microbarite cake. The pump was not powerful enough to build the pressue up to the operating value during filtration. The maximum pressure was not reached until the expression process was initiated. The curves for pressures of 3.4–24.7 MPa lie close to each other during filtration because of the limitation of the pump. The filtration and consolidation times are both on the

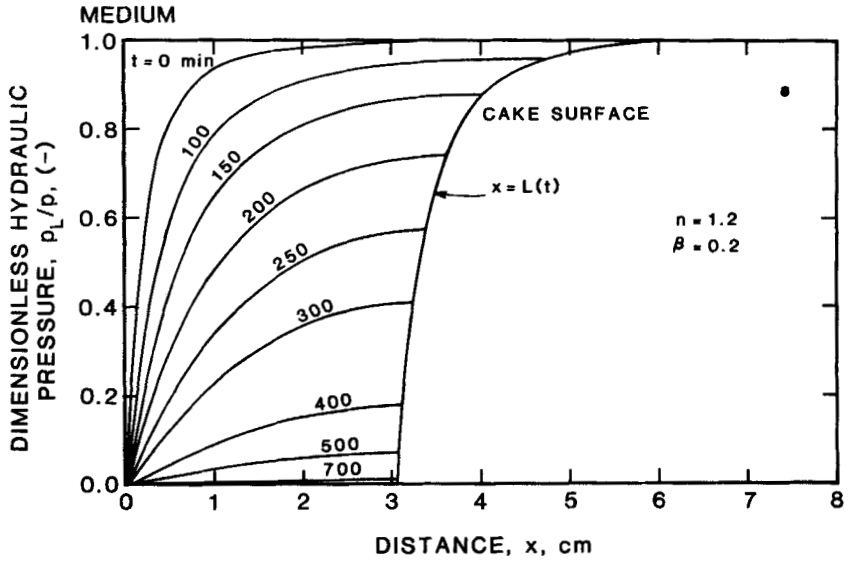

Figure 15a. Hydraulic pressure distribution in expression of a very highly compressible material.

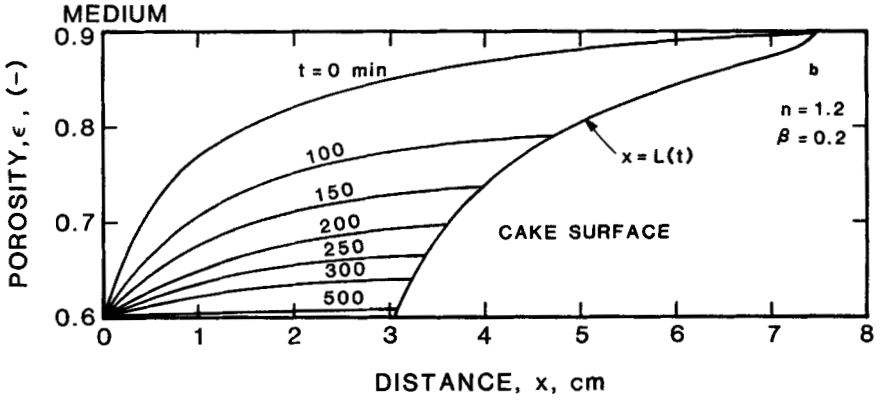

Figure 15b. Porosity distribution in expression of a very highly compressible material.

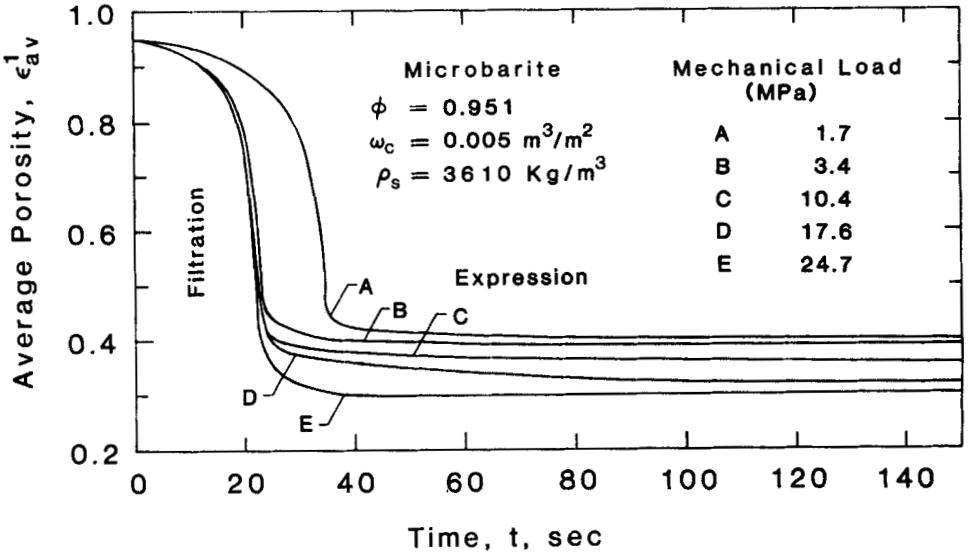

Figure 16. Average porosity vs. time in expression of microbarite.
Slurry conditions as in Table 1.

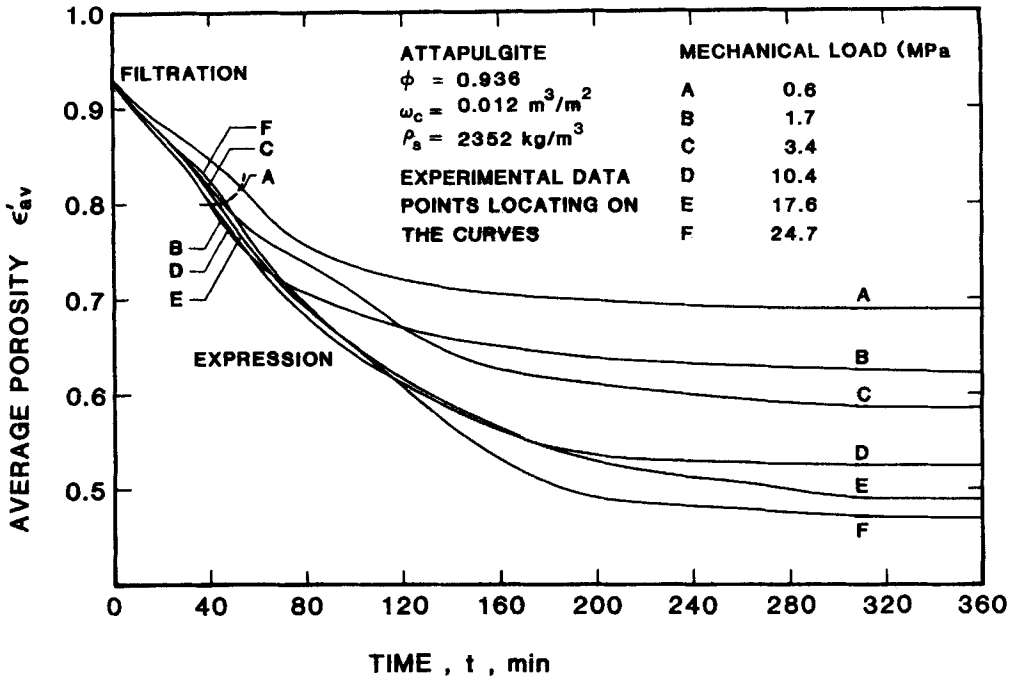

Figure 17. Average porosity vs. time in expression of attapulgite.
Slurry conditions as in Table 1.

order of 20 s. As the piston touches the cake surface, the solid particles that were under a null effective pressure during filtration start to bear the mechanical load directly, and the pressure at the cake surface increases to higher values.

The average porosity curves follow separate paths during consolidation. The rate of expression increases with pressure, and the final porosity is a function of the magnitude of the load placed on the piston. It is difficult to differentiate among the various curves because of the short times involved. The behavior is typical for a material of low compressibility and low resistance.

Experimental data for attapulgite are provided in Figure 17 for pressures ranging from 0.6 to 24.7 MPa. For this highly compressible material, the flow rate is not improved as the pressure is increased beyond 1.7 MPa during filtration. The filtration stage is completed in approximately 45 min for all pressures at which time expression begins. Since the early stage of consolidation is still controlled by the skin developed during filtration, the flow rate remains constant during the first portion of the expression process. Once the pressure gradient has dropped sufficiently, the rate of squeezing decreases, and the average porosity for each pressure in Figure 17 breaks away and approaches a limiting value. As the pressure is increased, the ultimate porosity decreases. Much longer filtration times of around 45 min and consolidation times of around 3h were encountered with attapulgite.

A theoretical treatment of the attapulgite-water system was made. Using constitutive equations for the data given in Figure 13 and the information in Table 1, the governing partial differential equation, Eq. 35, was solved by the methods of weighted residuals. The solutions were plotted in the same way as Figure 17; the results are shown in Figure 18. Comparing Figures 17 and 18, a reasonably good match between theoretical and experimental studies is seen to exist. The largest error occurs in the filtration period (first 45 min). There are two factors that principally account for the deviation. The first is sedimentation in the filtration process (Sambuichi et al., 1982). The second is uncertainty in the constitutive equations. The relationships of α with ϵ_s and p_s in the low-pressure region (e.g., smaller than 10 kPa) are difficult to measure precisely, especially for highly compressible materials. Extrapolating data from the high-pressure region leads to highly approximate results. The average porosity as given by Eq. 16 equals the ratio of two integrals, $\int_0^{\Delta p_c} dp_s/\alpha$ and $\int_0^{\Delta p_c} K dp_s$. Because the high flow resistance at high pressure leads to a rather small value of the reciprocal, the main contribution to the integrals arises in the low-pressure region (Tiller and Green, 1969). Therefore, knowledge of the constitutive equations in the low-pressure range is of primary importance in determining the average porosity of a highly compressible filter cake. On the other hand, the effective pressure grows throughout the cake during the expression period. The constitutive equation in the high-pressure range then becomes more impor-

Table 1. Properties of Slurries in Expression Tests

Material	Attapulgite + Water	Microbarite + Water
Solid density, kg/m^3	2,352	3,610
Mean particle size*, μm	4	10
Vol. dry solids per unit area ω_c, m^3/m^2	0.012	0.005
Vol. frac. solids in slurry ϕ_s	0.064	0.049

*As determined from sedimentation (Sedigraph). The irregular shape of the attapulgite particles affects settling rates.

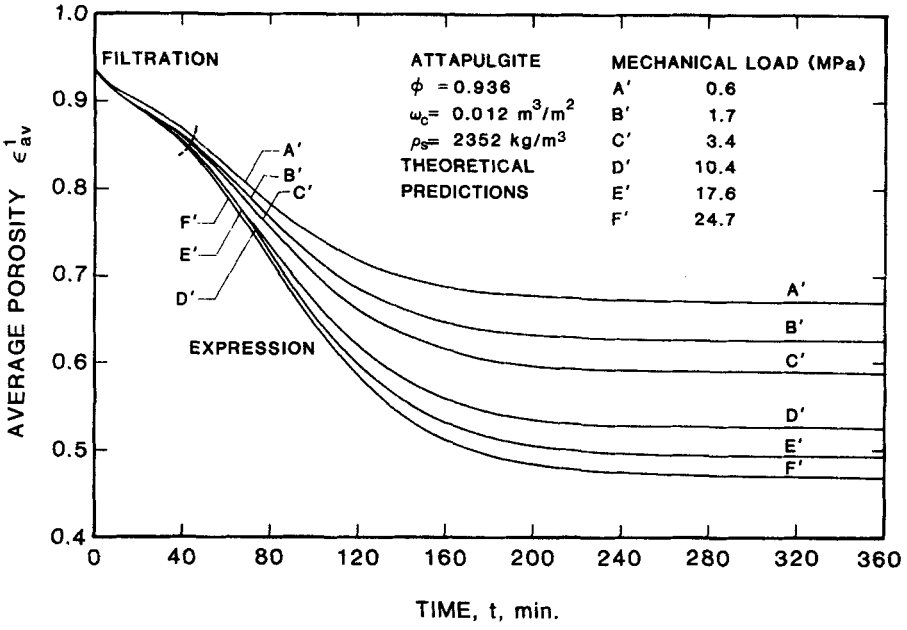

Figure 18. Theoretical prediction of average porosity vs. time in expression of attapulgite.

tant, and the constitutive equations in the low-pressure range are not required. A reasonable fit between theoretical predictions and experimental data was obtained for expression.

Acknowledgment

The authors thank the office of Basic Energy Sciences of the Department of Energy for Grant No. DE-AS05-81ER-10946, which has enabled them to carry on fundamental research in the theory of solid-liquid separation.

Notation

$A = \alpha/\alpha_o$
$E = \epsilon_s/\epsilon_{so}$
F_s = accumulative stress on particles lying in region from x to L, Pa
e = void ratio = $\epsilon/(1-\epsilon)$
K = permeability, m^2
K_{av} = average permeability, m^2
K_o = permeability of unstressed cake, m^2
L = cake thickness, m
M = dimensionless hydraulic pressure gradient at medium
n = compressibility coefficient, Eq. 2
$\bar{n}$ = unit normal to wavy surface
p = filtration or expression pressure, Pa
p_a = empirical constant, Eqs. 2–4, Pa
p_L = hydraulic pressure, Pa
p_s = effective or compressive pressure, Pa
Δp_c = hydraulic pressure across cake, Pa
$Q = q/q_\infty$
q = superficial velocity of liquid at an arbitrary point in cake, m/s
q_s = superficial velocity of solids at an arbitrary point in cake, m/s
q_t = superficial velocity of filtration at medium, m/s
q_∞ = limiting value of q at high pressure, m/s
R_m = medium resistance, m^{-1}
S = cross-sectional area, m^2
t = time, s
$T = \Delta p_c \epsilon_{so} t/\mu\alpha_o\omega_c^2$
u = absolute velocity of liquid, m/s
u_s = absolute velocity of solids, m/s
x = distance from medium, m

Greek letters

α = local specific flow resistance, m^{-2}
α_{av} = average specific flow resistance, m^{-2}
α_o = value of α in unstressed cake, m^{-2}
β = compressibility coefficient, Eq. 3
δ = compressibility coefficient, Eq. 4
ϵ = porosity
ϵ_{av} = average porosity
ϵ'_{av} = average volume fraction of liquid in expression cell
ϵ_s = volume fraction of solids (solidosity)
ϵ_{sav} = average volume fraction of solids
ϵ_{sl} = value of ϵ_s at medium
ϵ_{so} = unstressed value of ϵ_s
μ = liquid viscosity, Pa · s
$\Pi_L = p_L/p_a$
$\Pi_s = p_s/p_a$
$\Delta\Pi_c = \Delta p_c/p_a$
ρ_s = solid density, kg/m^3
ϕ_s = volume fraction of solids in slurry
$\Omega = \omega/\omega_c$
ω = volume of dry solids unit area between medium and any position in cake, m^3/m^2
ω_c = total volume/area of dry solids in cake, m^3/m^2

Literature cited

Aksay, D. S., "Microstructure Control through Colloidal Consolidation," *Advances in Ceramics. 10: Forming of Ceramics*, J. A. Mangles, ed. Am. Ceramic Soc., 94 (1984).
Chen, W., "A Study of the Mechanism of Sedimentation," M.S. Thesis, Univ. Houston (1984).
Grace, H. P., "Resistance and Compressibility of Filter Cakes," *Chem. Eng. Prog.*, **49**, 303 (1953).
Leu, W., "Cake Filtration," Ph.D. Diss. Univ. Houston (1981).
Masterton, F. R., "Pressure Profiles through Filter Cakes," M.S. Thesis, Univ. Houston (1979).
Okamura, S., and M. Shirato, "Liquid Pressure Distribution within Cakes in the Constant Pressure Filtration," *Kagaku Kogaku*, **19**, 104 (1955).
Okoh, B. O., "Studies in Filtration Characteristics of Particulate Systems," M.S. Thesis, Univ. Houston (1977).
Risbud, H. M., "Mechanical Expression, Stress at Cake Boundaries,

and New Compression-Permeability Cell," Ph.D. Diss., Univ. Houston (1974).
Sambuichi, M., H. Nakakura, and K. Osasa, "The Effect of Gravity Settling on Constant Pressure Filtration," *Mem. Fac. Eng. Yamaguchi Univ.*, **33,** 65 (1982).
Schiffman, R. L., V. Pane, and V. Sunara, "Sedimentation and Consolidation," *Proc. Flocculation, Sedimentation, Consolidation Conf.*, B. Moudgil and P. Somasundaran, eds., Eng. Found., New York, 57 (1986).
Shirato, M., M. Sambuichi, H. Kato, and T. Aragaki, "Internal Flow Mechanism in Filter Cakes," *AIChE J.*, **15,** 405 (1969).
Shirato, M., H. Kato, K. Kobayashi and H. Sakazaki, "Analysis of Settling of Thick Slurries Due to Consolidation," *J. Chem. Eng. Japan*, **3,** 1 (1970).
Smiles, D. E., "A Theory of Constant-Pressure Filtration," *Chem. Eng. Sci.*, **25,** 985 (1970).
———, "Constant-Rate Filtration of Bentonite," *Chem. Eng. Sci.*, **33,** 1355 (1978).
———, "Constant-Pressure Filtration: The Effect of a Filter Membrane," *Chem. Eng. Sci.*, **37,** 707 (1982).
Tiller F. M., and T. C. Green, "Role of Porosity in Filtration. IX: Skin Effect with Highly Compressible Materials," *AIChE J.*, **19,** 1266 (1973).
Tiller, F. M., and L. L. Horng, "Hydraulic Deliquoring of Compressible Filter Cakes. I: Reverse Flow in Filter Presses," *AIChE J.*, **29,** 297 (1983).
Tiller, F. M., and C. J. Huang, "Theory of Filtration Equipment," *Ind. Eng. Chem.*, **53,** 529 (1961).
Tiller, F. M., and M. Shirato, "The Role of Porosity in Filtration. VI: New Definition of Filtration Resistance," *AIChE J.*, **10,** 61 (1964).
Tiller, F. M., J. R. Crump, and F. Ville, "A Revised Approach to the Theory of Cake Filtration," *Proc. Int. Symp. Fine Particles Process.* v.2, P. Somasundaran, ed., Amer. Inst. Mining, Metall., Pet. Eng., New York (1980).
Tiller, F. M., S. Haynes, and W. Lu, "The Role of Porosity in Filtration. VII: Effect of Side-Wall Friction in Compression-Permeability Cells," *AIChE J.*, **18,** 13 (1972).
Tsai, C. D., "Theoretical and Experimental Studies in Filtration Mechanisms," M.S. Thesis, Univ. Houston (1983).
Villadsen, J., and M. L. Michelsen, *Solution of Differenial Equation Models by Polynomial Approximation*, Prentice-Hall, Englewood Heights, NJ (1978).
Willis, M. S. and I. Tosun, "A Rigorous Cake Filtration Theory," *Chem. Eng. Sci.*, **35,** 2427 (1980).
Willis, M. S., M. Shen, and K. J. Gray, "Investigation of the Fundamental Assumptions Relating Compression-Permeability Data with Filtration," *Can. J. Chem. Eng.*, **52,** 331 (1974).
Yeh, S. H., "Cake Deliquoring and Radial Filtration," Ph.D. Diss., Univ. Houston (1985).
Yoshioka, N., K. Ueda, and K. Miyosho, "Liquid Pressure Distribution for Filtration through Curved Leaves," *J. Chem. Eng. Japan*, **5,** 291 (1972).

Manuscript received Sept. 19, 1985, and revision received Jan. 27, 1987.